AGU100 ADVANCING EARTH AND SPACE SCIENCE

Geophysical Research Letters

RESEARCH LETTER
10.1002/2018GL077351

Special Section:
New understanding of the solar eclipse effects on geospace: The 21 August 2017 Solar Eclipse

The Lower Ionospheric VLF/LF Response to the 2017 Great American Solar Eclipse Observed Across the Continent

M. B. Cohen[1], N. C. Gross[1], M. A. Higginson-Rollins[1], R. A. Marshall[2], M. Gołkowski[3], W. Liles[4], D. Rodriguez[5], and J. Rockway[5]

[1]School of Electrical and Computer Engineering, Georgia Institute of Technology, Atlanta, GA, USA, [2]Department of Aerospace Engineering Sciences, University of Colorado Boulder, Boulder, CO, USA, [3]Department of Electrical Engineering, University of Colorado, Denver, CO, USA, [4]Independent Consultant, USA, [5]Space and Naval Warfare Systems Command, San Diego, CA, USA

Key Points:
- Solar eclipse of August 2017 impacted radio wave propagation through lower ionosphere (60-90 km)
- Array of VLF/LF radio receivers observed changes that strongly varied as a function of path geometry
- We observe reflective scattering from eclipse totality spot when transmitter and receiver are proximal to the spot

Correspondence to:
M. B. Cohen,
mcohen@gatech.edu

Citation:
Cohen, M. B., Gross, N. C., Higginson-Rollins, M. A., Marshall, R. A., Gołkowski, M., Liles, W., et al. (2018). The lower ionospheric VLF/LF response to the 2017 Great American Solar Eclipse observed across the continent. *Geophysical Research Letters*, *45*, 3348–3355. https://doi.org/10.1002/2018GL077351

Received 29 JAN 2018
Accepted 14 MAR 2018
Accepted article online 25 MAR 2018
Published online 24 APR 2018

Abstract We present observations from 11 very low frequency (VLF)/low-frequency (LF) receivers across the continental United States during the 21 August 2017 "Great American Solar Eclipse." All receivers detected transmissions from VLF/LF beacons below 50 kHz, while seven also recorded LF beacons above 50 kHz, yielding dozens of individual transmitter-receiver radio links. Our observations show two separable superimposed signatures: (1) a gradual rise and fall in signal levels visible on almost all paths as the eclipse advances and then declines, as VLF attenuation is reduced by the changing ionosphere under an eclipsed Sun, and (2) direct reflective scattering off the narrow 100-km-wide totality spot, observed more uniquely when the transmitter or receiver, if not both, are relatively close to the totality spot.

Plain Language Summary A solar eclipse provides a unique opportunity to study a region of the upper atmosphere known as the ionosphere, which is essentially the transition zone between Earth's atmosphere and the space environment. While the Sun is known to have a dominant impact on the electrical properties of this region, it is difficult to quantify it precisely since these altitudes, 60–90 km, are too high to reach with balloons yet too low for satellites. On the other hand, the lower ionosphere plays a key role in communications and navigation. Very low frequency/low-frequency radio waves at 3–300 kHz reflect from this region, thus allowing us to remotely diagnose the lower ionosphere. A solar eclipse is the only time when the Sun's influence rapidly turns off over a very small region. In this paper, we have analyzed dozens of diagnostic observations, namely, transmitter-to-receiver communications links, that allow to quantify how the lower ionosphere responded to this unique geophysical event. As the Sun's influence changes, so too does the characteristics of these very low frequency/low-frequency transmitters detected many hundreds to thousands of miles away.

1. Introduction

The lower ionosphere (between 60 and 90 km), known as the *D* region, is dominantly impacted by the Sun's radiation during daytime. There remains uncertainty in the characteristics of the *D* region as a function of season, latitude, and sunspot number. The *D* region is an area where the International Reference Ionosphere (Bilitza et al., 2011) has much less accuracy. An effective way to monitor the *D* region is through the use of very low frequency (VLF, 3–30-kHz) and low-frequency (LF, 30–300-kHz) radio waves, which unlike higher frequencies reflect efficiently from the *D* region and are thus guided to global distances in the "Earth-ionosphere waveguide." As such, VLF/LF remote sensing is a valuable tool to probe a wide variety of ionospheric changes from lightning heating, electron precipitation, solar flares, gamma rays, and other phenomena (see reviews by Barr et al., 2000; Inan et al., 2010).

It is unsurprising that the *D* region responds to a solar eclipse, when some or all of the Sun's influence is blocked. Schledermann (1912) noted an effect on telegraph signals at 375 kHz. Burton and Boardman (1933) provided a first account of VLF/LF propagation effects when the electromagnetic signature of lightning-generated radio atmospherics changed substantially. More quantitative analysis in modern times has led to ionospheric characterization using the "tweek" signature, which ordinarily only appears during the nighttime hours (Rycroft & Reeve, 1970; Singh et al., 2011).

A larger number of papers have looked at VLF/LF beacons as a method to infer ionospheric changes. Kaufmann and Schaal (1968) and Schaal et al. (1970) presented VLF observations of the 12 November 1966 eclipse over South America, finding that the NPM transmitter (then at 26.1 kHz) from Hawaii was delayed by 10 μs (or 94°). Hoy (1969) noted VLF phase delays of ~3.3 μs (19°) during 22 September 1968 eclipse over Asia, on an extremely long 17-Mm path from Rugby, UK, to Canberra, Australia, at 16 kHz. Da Costa et al. (1995) presented variations of the "Omega" transmitters (Swanson, 1983) during the 30 June 1992 eclipse over South America. Kozlov et al. (2007) examined the 29 March 2006 eclipse over Africa and Asia. Theoretical efforts have proceeded based on these measurements. Lynn (1981) cataloged observations of the 23 October 1976 eclipse over the Indian Ocean on Omega transmitters and applied an Omega diurnal correction model to derive ionospheric response time constants. Clilverd et al. (2001) examined an extensive set of observations from five receivers and four VLF transmitters during the 11 August 1999 eclipse over Europe. For short and medium paths, amplitude variations were positive with some sharp negative deviations, while for longer paths they were generally negative. Accompanying theoretical calculations with the long wavelength propagation capability model (Morfitt & Shellman, 1976) in many cases lined up with the observations for an assumed ionospheric profile. A homogeneous electron density was assumed along the entire path, so the ionospheric variation was larger for shorter paths, which loosely captures the spatial variation of the ionospheric impact.

Observations of transmitter signals in the LF band have also been made. LF propagation is not as efficient as VLF, but beacons can nonetheless be detected even thousands of kilometers away (Higginson-Rollins & Cohen, 2017). Doherty (1970) observed 100-kHz LORAN-C pulses in Alaska during the July 1963 solar eclipse and found a phase change and a recovery overshoot. Buckmaster and Hansen (1986) examined the effect of the 26 February 1979 eclipse over the northwest United States on the WWVB timing signal at 60 kHz from Colorado, finding a decline of 1–2 μs, or 21–43°. Bamford (2000) examined the 11 August 1999 eclipse over Europe, including its effects on the 75-kHz timing signal from Switzerland. At various observation sites, there was a wide variety of signal types, including a slow rise/fall and a "w" shape.

We present here a set of *D* region diagnostics at both VLF and LF frequencies for the total solar eclipse of 21 August 2017, focused on beacons at or below 60 kHz.

2. Description of Data and Processing

The Great American Solar Eclipse occurred on 21 August 2017. The totality spot, in this case ~100-km wide, is where the Moon fully covers the Sun. On the ground, it appeared over the Pacific Ocean at 16:48:32 UT and ended over the Atlantic Ocean at 20:01:35 UT. It cut across the continental United States from northwest to southeast, taking ~90 min to cross the continent.

To observe the ionospheric impact of the eclipse, data were collected from two versions of a radio receiver known as the Atmospheric Weather Electromagnetic System for Observation Modeling and Education (AWESOME). The receiver consists of typically two orthogonal air-core loop antennas to sample the horizontal components of the magnetic flux density. Typically, we have one antenna sensitive to signals arriving from the north-south direction and another sensitive to signals arriving from the east-west direction. The receivers have Global Positioning System timing synchronization and 16 bits of dynamic range. Both have magnetic flux density spectral sensitivity of 0.03–0.3 fT/rt-Hz and so are limited primarily by atmospheric and cultural noise. Both can save broadband magnetic flux density data or extract the amplitudes and phases of narrowband beacon signals in real time. The original version of the AWESOME (VLF version) was built at Stanford University and is described by Cohen et al. (2010). It consisted of an analog-to-digital converter that sampled at 100 kHz, timing accuracy of 100 ns, and captured the spectrum between 300 and 47 kHz. An upgraded version of the AWESOME (LF version) is built at Georgia Tech. The newer version improves the timing accuracy to <20 ns and utilizes a faster 1-MHz analog-to-digital converter to capture the radio spectrum between 500 and 470 kHz, with improved sensitivity. Calibration is achieved by injecting a known signal into the front end of the preamplifier, which, via Faraday's law, corresponds to a magnetic flux density value given the size of the antenna and number of turns.

We utilize data from 11 AWESOME receivers in the continental United States or Canada that operated during the solar eclipse, which are shown in Figure 1. Seven of these receivers (blue squares) are of the more recent LF AWESOME version and are built and operated by Georgia Tech. These are the receivers in Dover (39.28°N, 75.58°W), PARI (35.20°N, 82.87°W), Briarwood (33.43°N, 82.58°W), Baxley (31.88°N, 82.36°W),

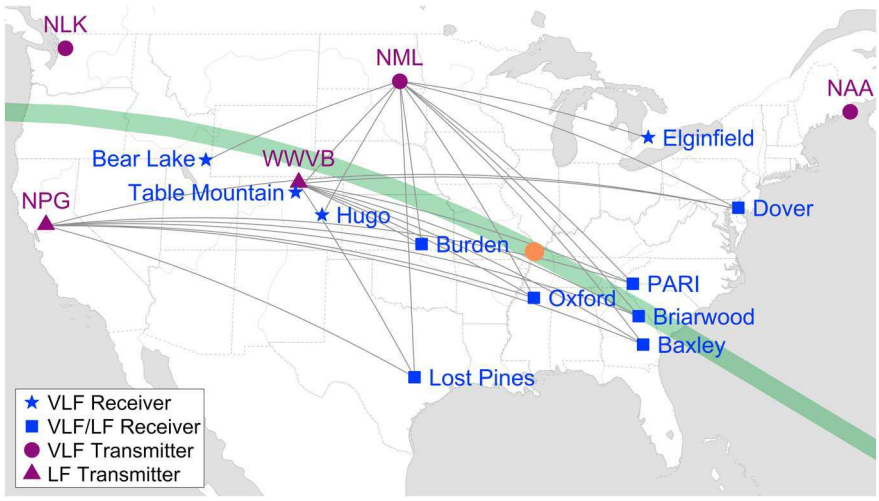

Figure 1. Map of observations. Very low frequency (VLF) or low-frequency (LF) transmitters are shown as maroon circles, VLF or LF receivers as shown with blue stars. The green swath shows the path of the eclipse totality spot (from northwest to southeast) at 80-km altitude. The orange spot is the location with the longest totality duration (2 min, 41 s), which occurred at 18:21:49 UT. Gray lines show great circle paths from transmitters to receivers that were recorded.

Lost Pines (30.09°N, 97.17°W), Oxford (34.43°N, 89.39°W), and Burden (37.32°N, 96.75°W). Three receivers (blue squares) are the original VLF AWESOME version and operated by the University of Colorado Boulder. These are located at Bear Lake (41.93°N, 111.42°W), Table Mountain (40.13°N, 105.24°W), and Elginfield (43.19°N, 81.32°W). The remaining receiver (blue square), in Hugo (38.89°N, 103.41°W), is similar to the original VLF AWESOME with some additional differences, built and operated by the University of Colorado Denver.

We monitor the signals from three transmitters, used by the U.S. Navy for submarine communications with 200-baud minimum shift keying (MSK), shown with maroon circles (VLF) and triangles (LF) in Figure 1. The NML transmitter operates at 25.5 kHz and is located at 46.37°N, 98.34°W). The official call sign is actually NTD although in the academic literature it is generally referred to as NML or NLM. Two other U.S. Navy VLF transmitters were not operating on the day of the eclipse, NAA and NLK, but are shown anyway. NPG is a U.S. Navy VLF/LF transmitter that was specially keyed for this event at 55.5 kHz and 135.95 kHz. We detected both transmission frequencies, although here we present only 55.5 kHz. NPG operates with a 200-baud MSK with a known bit repeating sequence: 1-1-0-0. Finally, the WWVB timing beacon, operated by the U.S. National Institute of Standards and Technology agency (40.68°N, 105.05°W), broadcasts at 60 kHz with amplitude modulation and binary phase shift keying.

The seven LF AWESOME receivers operated by Georgia Tech captured the two >50-kHz transmitters (NPG and WWVB), whereas the other four only recorded NML. The map in Figure 1 shows paths for all transmitter-receiver links that were monitored during the eclipse day and included in this work.

The 200-baud MSK modulation must be removed in order to extract the phase. Our algorithm to achieve this is described in Gross et al. (2018). For the Georgia Tech receivers, this algorithm was applied in real time; for the others it was applied in postprocessing of the collected broadband data. MSK demodulation has a 90° ambiguity when the MSK code history is not known. Our algorithm described by Gross et al. (2018) synchronizes the MSK demodulation between two antenna signals, so that the phase difference between the two is still reliable even with the 90° ambiguity. This step enables polarization calculations, in which we take the two magnetic flux density directions, we rotate them such that one channel is along the radial direction from the source, and then we determine the major axis, minor axis, tilt angle, and start phase of the ellipse. Polarization measurements require accurate antenna calibration and orientation information. For the seven Georgia Tech receivers and the CU-Denver receiver these are available and have been applied. However, calibration for the three CU-Boulder receivers was not available. We estimated rough proportional conversion factors so that the magnetic flux density from those receivers is consistent with the others.

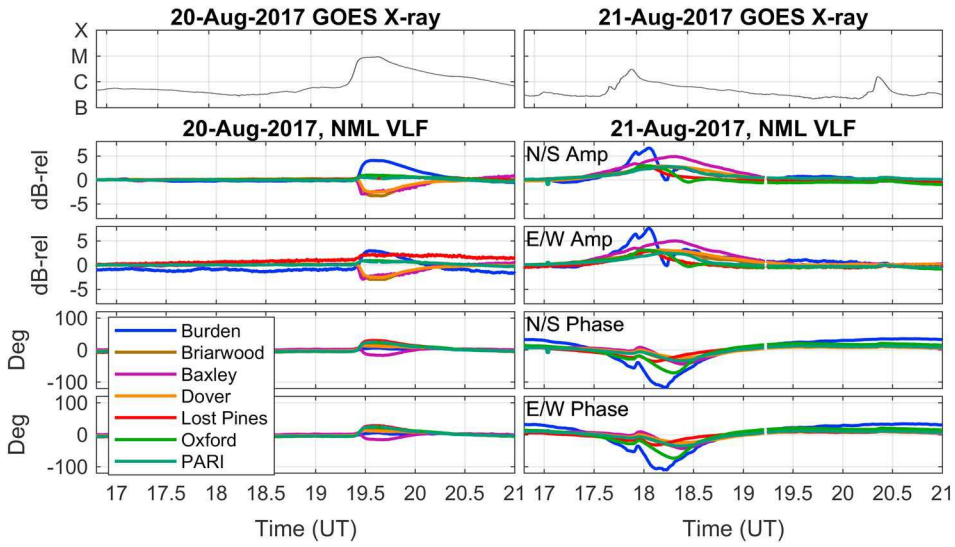

Figure 2. Observations at six selected receivers on the day before (left) and the day of (right) the eclipse. The four rows correspond to the four signal channels (north-south, N/S antenna amplitude, east-west, E/W antenna amplitude, N/S antenna phase, E/W antenna phase). VLF = very low frequency.

3. Baseline and Solar Flares

The ionospheric propagation conditions are typically very steady during the daytime, showing only gradual changes with the solar zenith angle (Han & Cummer, 2010; Thomson, 1993), with notable exception when a solar flare occurs. Figure 2 shows the raw data of NML recorded at the seven LF receivers, during the period 16:48–21:00 UT on both 20 August (left) and 21 August (right). For reference, the GOES-14 X-ray flux is shown in the first row. The next four rows show the amplitude (in dB) of the north-south (N/S) antenna, the amplitude of the east-west (E/W) antenna, then N/S phase (degrees) and E/W phase. We have equalized the VLF amplitudes and phases at all the sites so that deviations can be visually noted, so these values are uncalibrated.

The eclipse effect is very clear between 1745 and 1845 on 21 August. However, the analysis is complicated some by the presence of a solar flare with modest intensity (C4) roughly between 1745 and 1805 UT, peaking at 1755 UT. Since the ionosphere responds and recovers quickly compared to the solar flux changes, we can determine a threshold flux level beyond which VLF propagation conditions are disturbed (and below which they are not). To do this, we utilize two other solar flares. The first occurred on 20 August at 1930 UT, a powerful M1 flare whose effects on VLF propagation are obvious in the left column of Figure 2. There is an amplitude change (up or down) as much as 4 dB at each site when the solar flare hits. Close examination of the rise of the solar flare indicates that VLF signals are significantly impacted starting at roughly the C3 intensity for these paths and season, suggesting that C3 is a good threshold for VLF disturbance. This suggestion is confirmed by a second weaker solar flare, which reached the C1 level at 2020 UT on 21 August shortly after the eclipse, whose effects are barely visible in the data.

We can therefore say that the solar flare during the eclipse had a fairly small effect on our observations, since it reached the C4 level, barely exceeding the C3 threshold and for only a brief period. In the Burden signal, the effect of this solar flare can be seen as the small peak that occurs shortly before 18 UT, coincident with the solar flare peak. Similar or smaller variations appear on other receivers. Since the ionosphere recovers quicker than the characteristic rise and fall time of the solar flare, we assume that the solar flare has no additional impact on VLF propagation.

4. Eclipse VLF and LF Observations

Our observations for all 11 operating receivers during the eclipse for the NML receiver are shown in Figure 3. The data are calibrated and displayed as polarization ellipses, as described by Gross et al. (2018). To emphasize slower changes associated with the solar flare and solar eclipse, we apply a 60-point median filter to the data set, which is applied on top of low-resolution 1-s data. The median filter mitigates impulses from intense lightning radiation. The columns correspond to the different receivers, and the rows to the four polarization

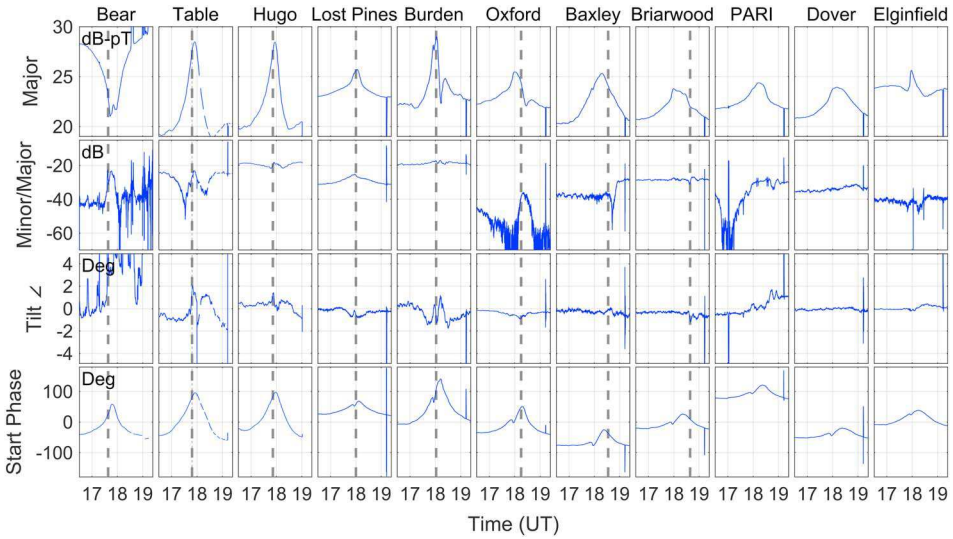

Figure 3. Polarization observations of NML (25.2 kHz) at all 11 receivers (each in a column) between 1630 and 1920 UT on 21 August, during the eclipse.

properties. Magnetic flux density units of dB-pT are shown for the first row, and the second row is the ratio of the major axis to the minor axis, in dB. The third row is tilt angle and is displayed as degrees counterclockwise with respect to the azimuthal direction. Tilt angle can be thought of as the error in measured arrival angle compared to the actual arrival angle. Generally, terrain effects and slight antenna misalignment cause the apparent arrival direction to differ from the actual direction by as much 5°, although this can be inferred and then removed by observing lightning-generated sferics at many arrival angles (Gross et al., 2018; Wood & Inan, 2002; Zoghzoghy et al., 2015). Here we remove this few degree effect manually, as we are interested not in the ambient tilt angle but how it changes. The fourth row is start phase, which captures phase changes that occur on both antennas simultaneously. If the transmitter-receiver path crossed the eclipse totality path, a vertical gray line indicates the time of peak eclipse.

The 11 rows are sorted from west to east or by chronological order that the eclipse totality spot passed over the transmitter-receiver path. The paths from NML to several of the receivers go only a couple hundred kilometers beyond the totality path, including Bear Lake, Table Mountain, Hugo, Burden, Oxford, and Baxley. The paths from NML to PARI ends just short of the totality path. NML to Lost Pines path goes significantly past the totality

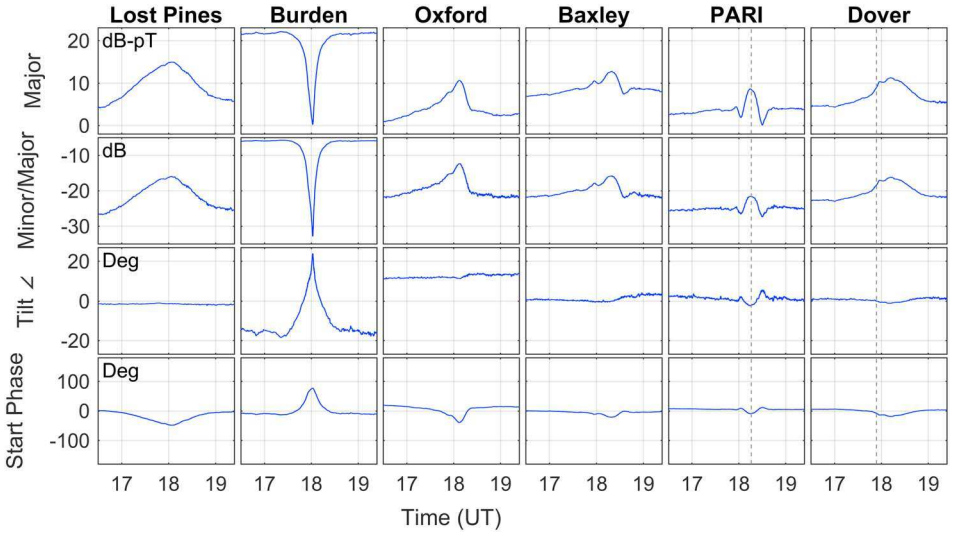

Figure 4. Same as Figure 3 but for the WWVB transmitter signal at 60 kHz and only for the seven low-frequency receivers.

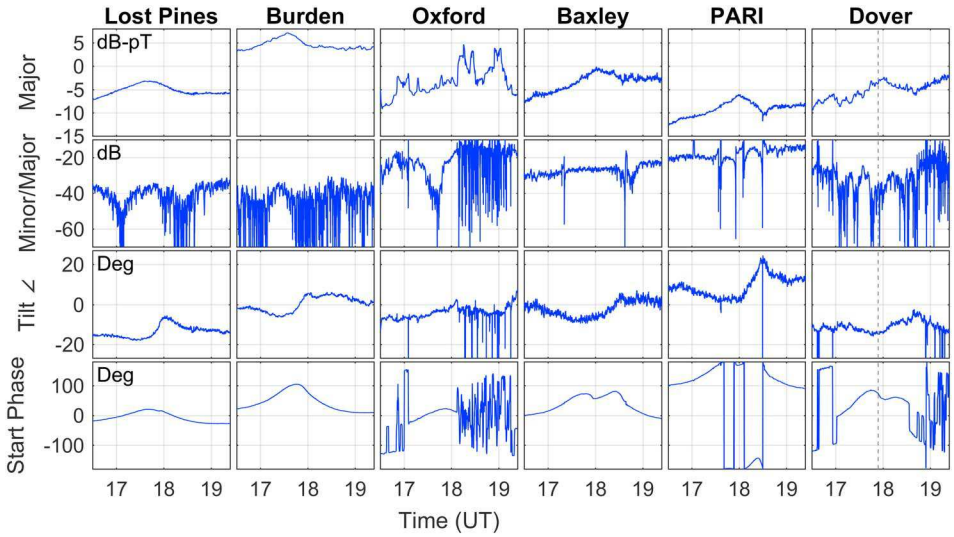

Figure 5. Same as Figure 4 but for the NPG transmitter signal at 55.5 kHz.

path. The NML to Elginfield and Dover paths traverse only a partial eclipse. Vertical gray lines indicate when the totality occurred along the transmitter-receiver path, if applicable.

A gradual rise in the signal amplitude is clearly evident in most of the paths. This occurs at all receivers, even Dover and Elginfield, which are only partially eclipsed. One notable exception to this is Bear Lake, which actually shows a descending amplitude followed by a recovery. One of the sites, Burden, also stands out due to a sharp minimum in the major axis length evident shortly after 18 UT. This minimum is also evident but less intense at Oxford and Hugo.

The second row of Figure 3 indicates the ratio between the minor and major axis lengths. Zero decibel indicates circular polarization, whereas a very high ratio indicates linear polarization. For daytime VLF propagation at medium and long range, the polarization tends to be highly linear (Gross et al., 2018). Many of the sites displayed here do not show a significant shift in the major/minor ratio, indicating that the shape of the polarization ellipse does not change appreciably. Two notable exceptions are Bear Lake and Oxford, both of which show a ~20-dB shift toward circular polarization, while Oxford shows a 20-dB shift toward linear polarization. The presence of circular polarization arises from the mix of quasi-transverse electric and quasi-transverse-magnetic modes, although in general the quasi-transverse-magnetic modes dominate. At Oxford and PARI, the NML signal is so close to linearly polarized that the minor axis cannot be detected with high signal-to-noise ratio.

The third row indicates that for the most part, the polarization tilt angle does not appreciably change, with the notable exceptions of Hugo and Burden, for which the ellipse rotates by a few degrees during the eclipse. The fourth row looks very similar at the sites, namely, an advance in the phase during the rise of the eclipse, followed by a decline. As the start phase is connected to the total phase change from transmitter to receiver, we interpret this to mean that the average phase velocity along the path decreased during the eclipse. We note that phase velocity is only strictly connected to measured phase when a single mode dominates the signal, and in multimode propagation environment the phase may go up or down depending on the constructive and destructive interference of the individual modes. However, it is notable here that at all 11 sites, the phase advances and then declines with the eclipse. This suggests that the change in ionospheric attenuation rate (dB/Mm) may be more directly observable than in ordinary multimode conditions, either because a single mode is dominant or that the attenuation rate and phase velocity of all propagating modes are affected by roughly the same amount.

Observations from two LF transmitters NPG and WWVB are now analyzed, for the seven LF AWESOME receivers. NPG and WWVB are at a similar frequency, but NPG is further to the west, away from the receivers and the eclipse totality path. Figure 4 shows the polarization observations for WWVB. Most of the sites show

the same slow rise and slow fall in the major axis amplitude, described earlier for NML observations. Like the NML observations, Burden shows very distinct characteristics. There is also some extra fluctuation at PARI and even Baxley.

Figure 5 shows the polarization observations for NPG. As NPG is further away from the receivers than WWVB and has comparable radiated power, the signals are significantly weaker. At most sites there is a gradual rise and fall in the major axis, although at Oxford the data set is very noisy. The polarization ellipse also changes significantly in angle during the eclipse passage. The start phase also advances at most sites, with a curious double-hump visible at the east coast sites (Baxley, Dover, and PARI) that is not apparent in the central United States sites (Lost Pines, Burden, and Oxford).

5. Discussion and Conclusion

In general, the variation in VLF/LF propagation during a solar eclipse varies greatly with path length, angle, and location of to the totality spot with respect to the path, frequency, and other parameters. This is well known, the most extensive work to date on this having been done by Clilverd et al. (2001).

Our observations here, though, reveal what we interpret to be two separable effects. The first is a gradual shift in propagation conditions owing to the reduction in the input solar flux (extreme ultraviolet and Lyman-alpha radiation) onto the ionosphere, even under a partial eclipse. By gradual, we mean on the scale of the entire eclipse event: many to tens of minutes and many hundreds of kilometers. Although the fraction of the solar flux blotted out varies with distance, there is no sharp gradient to this change, so VLF/LF propagation essentially continues with a gradually shifting attenuation rate and/or phase velocity. This effect is similar to what happens when a solar flare impacts the entire ionosphere (Thomson & Clilverd, 2001). In most of our observations this manifests as a gradual rise and then decline in the signal strength.

A second effect, experimentally separable, is the direct reflective scattering of signals from the eclipse totality spot itself. In addition to a slow rise and fall of the signal strength, certain paths demonstrate specific characteristics only during the totality passage, including (1) rotation back and forth multiple times of the polarization ellipse and (2) brief sharp fall in amplitude (on top of the gradual increase). For most of the eclipse, the shadow of the Moon was roughly circular or oblong with a 100-km diameter. This is only modestly wider than the 50-km diameter of a typical early/fast event (Johnson et al., 1999). Within this region, the ionosphere is changing very rapidly in both space and time, as the complete absence of solar input drives down the electron density on a timescale of a minute or so, due to recombination and attachment processes. The maximum eclipse duration of 162 s is long enough to allow the ionosphere to settle much closer to a nighttime state. With sharp spatial gradients present, VLF/LF propagation is affected by modal conversion in and near the eclipse totality spot, as is also known to occur during the day/night terminator passage. The observations are more easily affected by mode conversion as the following three conditions are true: (1) the transmitter is relatively close to the eclipse totality spot, (2) the receiver is close to the totality spot, and (3) the frequency is higher.

Mode conversion is most effective when higher order modes (with a higher angle of incidence) still exist. On the other hand, the modes generated have relatively high attenuation rates, so are more easily observed when the receiver is not too far from the totality spot. Finally, shorter wavelengths have more electrical distance within the totality spot itself. For this reason, the scattering and mode conversion effect is mostly visible on certain transmitter-receiver paths, namely, NML to Burden, and to a lesser extent Hugo and Oxford, and WWVB to Burden and to a lesser extent PARI. The observed VLF/LF characteristics result from interference between ambient and newly created scattered modes.

Complete simulations may be able to confirm the separable nature of these two effects, via modeling the solar flux input, ionospheric *D* region chemistry, and VLF/LF propagation. We propose that this direct reflective scatter would not be present during, for example, a partial solar eclipse. So such a simulation could be repeated for identical geometry, once with 100% peak eclipse and once with a 99% peak eclipse, and these may show markedly different predictions for certain paths. Although we cannot state whether the totality zone reaches nighttime conditions, we can say that VLF observations indicate a much more abrupt change to the ionospheric properties within that region.

Acknowledgments
This work was supported by the National Science Foundation under grant AGS 1451142 and 1653114 (CAREER) to Georgia Tech, by grant AGS 1451210 to the University of Colorado Denver, and by NASA grant NNX17AI05G to the University of Colorado Boulder. Data are available at doi:10.5281/zenodo.1195781. We thank the various site hosts for helping maintain our equipment. We thank the team at NPG in Dixon, CA, for arranging special broadcast during the solar eclipse. We thank Jackson McCormick, Parker Singletary, Lee Thompson, and Nate Opalinski for help taking the Georgia Tech measurements and Jamie Bittle, Poorya Hosseini, Chad Renick, and J. B. Rudsill for help with the CU-Denver Hugo measurements.

References

Bamford, R. (2000). Radio and the 1999 UK total solar eclipse (Tech. Rep.). Radiocommunications Agency. Radio Communication Research Unit, Rutherford Appleton Laboratory, Chilton, Didcot, UK.

Barr, R., Llanwyn Jones, D., & Rodger, C. J. (2000). ELF and VLF radio waves. *Journal of Atmospheric and Solar-Terrestrial Physics*, *62*, 1689–1718.

Bilitza, D., McKinnell, L.-A., Reinisch, B., & Fuller-Rowell, T. (2011). The international reference ionosphere today and in the future. *Journal of Geodesy*, *85*(12), 909–920. https://doi.org/10.1007/s00190-010-0427-x

Buckmaster, H. A., & Hansen, S. (1986). 26 february 1979 total solar eclipse induced LF (60 kHz) phase retardations. *Journal of Atmospheric and Terrestrial Physics*, *48*(4), 393–397.

Burton, E. B., & Boardman, E. M. (1933). Effects of solar eclipse on audio frequency atmospherics. *Nature*, *129*, 81.

Clilverd, M. A., Rodger, C. J., Thomson, N. R., Lichtenberger, J., Steinback, P., Cannon, P., & Angling, M. J. (2001). Total solar eclipse effects on VLF signals: Observations and modeling. *Radio Science*, *36*(4), 773–788.

Cohen, M. B., Inan, U. S., & Paschal, E. P. (2010). Sensitive broadband ELF/VLF radio reception with the AWESOME instrument. *IEEE Transactions on Geoscience and Remote Sensing*, *48*(1), 3–17. https://doi.org/10.1109/TGRS.2009.2028334

Da Costa, A. M., Paes Leme, N. M., & Rizzo Piazza, L. (1995). Lower ionosphere effect observed during the 30 June 1992 total solar eclipse. *Journal of Atmospheric and Terrestrial Physics*, *57*(1), 13–17.

Doherty, R. J. (1970). Comparison of 100 kHz pulse propagation during two solar eclipses. *Nature*, *226*, 1129.

Gross, N. G., Cohen, M. B., Said, R. K., & Golkowski, M. A. (2018). Polarization measurements of VLF transmitters as an ionospheric diagnostic. *Journal of Geophysical Research: Space Physics*, *123*, 901–917. https://doi.org/10.1002/2017JA024907

Han, F., & Cummer, S. A. (2010). Midlatitude daytime *D* region ionosphere variability measured from radio atmospherics. *Journal of Geophysical Research*, *115*, A10314. https://doi.org/10.1029/2010JA015715

Higginson-Rollins, M. A., & Cohen, M. B. (2017). Exploiting LF/MF signals of opportunity for lower ionospheric remote sensing. *Geophysical Research Letters*, *44*, 8665–8671. https://doi.org/10.1002/2017GL074236

Hoy, R. F. (1969). The effect of a total solar eclipse on the phase of long path v.l.f. transmissions. *Journal of Atmospheric and Terrestrial Physics*, *31*, 1027–1027.

Inan, U. S., Cummer, S. A., & Marshall, R. A. (2010). A survey of ELF/VLF research on lightning-ionosphere interactions and causative discharges. *Journal of Geophysical Research*, *115*, A00E36. https://doi.org/10.1029/2009JA014755

Johnson, M. P., Inan, U. S., Lev-Tov, S. J., & Bell, T. F. (1999). Scattering pattern of lightning-induced ionospheric disturbances associated with early/fast VLF events. *Geophysical Research Letters*, *26*(15), 2363–2366.

Kaufmann, P., & Schaal, R. E. (1968). The effect of a total solar eclipse on long path VLF transmissions. *Journal of Atmospheric and Terrestrial Physics*, *30*, 469–471.

Kozlov, V. I., Karimov, R. R., & Mullayarov, V. A. (2007). Observation of signals of VLF radio stations and VLF noise during the solar eclipse on March 29, 2006. *Russian Physics Journal*, *50*(6), 617–620.

Lynn, K. (1981). The total solar eclipse of 23 October 1976 observed at VLF (*Technical report erl-0093-tr*). Defense Science and Technology Organization. Australian Defence Scientific Service, Defence Research Establishment, Salisbury, South Australia.

Morfitt, D. G., & Shellman, C. H. (1976). MODESRCH, An improved computer program for obtaining ELF/VLF/LF mode constant in an Earth-ionosphere waveguide (*Westinghouse Report, 80133F-1*). submitted to the Office of Naval Research. San Diego, CA: Naval Electronics Lab Center.

Rycroft, M. J., & Reeve, C. D. (1970). VLF radio signals observed in Newfoundland during the solar eclipse of March 7, 1970. *Nature*, *226*, 1126–1127.

Schaal, R. E., Mendes, A. M., Ananthakrishnan, S., & Kaufmann, P. (1970). VLF propagation effects produced by the eclipse. *Nature*, *226*, 1127–1128.

Schledermann, H. (1912). Effect of the solar eclipse on wireless telegraph signals. *The Electrician*, *May 31*, 329.

Singh, R., Veenadhari, B., Maurya, A. K., Cohen, M. B., Kumar, S., Selvakumaran, R., et al. (2011). *D*-region ionosphere response to the total solar eclipse of 22 July 2009 deduced from ELF/VLF tweek observations in the Indian sector. *Journal of Geophysical Research*, *116*, A10301. https://doi.org/10.1029/2011JA016641

Swanson, E. R. (1983). Omega. *Proceedings of the IEEE*, *71*(10), 1140–1155.

Thomson, N. R. (1993). Experimental daytime VLF ionospheric parameters. *Journal of Atmospheric and Terrestrial Physics*, *55*, 831–834.

Thomson, N. R., & Clilverd, M. A. (2001). Solar flare induced ionospheric *D*-region enhancements from VLF amplitude observations. *Journal of Atmospheric and Solar-Terrestrial Physics*, *63*, 1729–1737.

Wood, T. G., & Inan, U. S. (2002). Long-range tracking of thunderstorms using sferic measurements. *Journal of Geophysical Research*, *107*(D21), 4553.

Zoghzoghy, F. G., Cohen, M. B., Said, R. K., Lehtinen, N. G., & Inan, U. S. (2015). Ship-borne LF oceanic lightning observations and modeling. *Journal of Geophysical Research: Atmospheres*, *120*, 10,890–10,902. https://doi.org/10.1029/2015JD023266